Supporting Information

High Zn(002)-preferential orientation enabled by proton additive for dendrite-free zinc anode

Yating Li, Xiaohui Ma, Xi Zhang, Fengyi Zhang, Qiang Guo, Jinlong Liu, Yonggang Wang, Jianhang Huang, * Yongyao Xia*

Experimental Section

Materials

$ZnSO_4 \cdot 7H_2O$ (AR) was purchased from Aladdin Chemicals. H_2SO_4 (AR) and Na_2SO_4 (AR) were purchased from Sinopharm Chemical Reagent Co. Cu foil (99.99%), Ti foil (99.99%), stainless steel (SS) foil (99.99%) and Zn foil (99.99%) were purchased from Shengshida metal materials of China. PTO was prepared according to the previously reported method[1]. 5 g (25.4 mmol) pyrene (≥99.0%, Sigma-Aldrich) was added into 100 mL acetonitrile (≥99.0%, Sigma-Aldrich) and 100 mL CH_2Cl_2 (≥99.9%, Sigma-Aldrich). Then, 44.5 g (207.9 mmol) $NaIO_4$(⩾99.8%, Sigma-Aldrich), 125 mL H_2O and 0.64 g (3.1 mmol) $RuCl_3 \bullet xH_2O$(⩾99.98%, Sigma-Aldrich) were added successively. The dark brown mixture was heated at 40 °C overnight, and then remove the organic solvent through rotary evaporation treatment. After the solid are rinsed with H_2O and filtered, and dried in 70°C air to make a dark green cake. The pure golden needle-like product PTO was obtained going through column chromatography (using CH_2Cl_2 as mobile phase).

Preparation of the Zn(002)-textured electrode

The electrodeposition of Zn was performed using a three-electrode electrolytic cell with Cu foil (or SS, Ti foil) as the working electrode (i.e. deposition substrate), Saturated calomel electrode (SCE) as reference electrode, and Zn foil as the counter electrode. The distance between the working electrode and counter electrode was fixed to be 1.5 cm. To obtain (002) texture, 1 M $ZnSO_4$ + H_2SO_4 (from 0.05 to 1 M) electrolyte was used as electrolyte. The whole piece working electrode (Cu, SS or Ti) was covered with shielding tape, only leaving 1 cm^2 area exposed for electroplating. The electrodeposition was performed using galvanostatic procedure at 10 mA cm^{-2} or 55 mA cm^{-2}, or potentiostatic procedure at −1.2 V vs. SCE, and the deposition area capacity is 40 mAh cm^{-2}.

Materials characterizations

XRD patterns were recorded by an x-ray diffractometer (D8 Advance from Bruker AXS) with Cu Kα radiation (λ = 0.15406 nm). SEM images were obtained on field-emission Zeiss SEM Gemini 300 Scanning Electron Microscope. EBSD was conducted using JSM-7900F SEM coupled with an Oxford Nordlys max3 EBSD detector. The in-situ characterization of Zn deposition behavior was conducted on an optical microscope (Yuescope Co.) equipped with a digital camera. The relative texture coefficients (RTCs) of Zn metal were calculated according to the following formula:

$$RTC_{(hkl)} = \frac{I_{(hkl)}/I_{0(hkl)}}{\sum I_{(hkl)}/I_{0(hkl)}} \times 100\%$$

where $I_{(hkl)}$ is the diffraction intensity obtained from the deposited Zn, and $I_{0(hkl)}$ is the diffraction intensity of the standard Zn sample (PDF#01-1238).

Electrochemical characterizations

Electrochemical performances were evaluated using CR-2016 coin-type cells, in which glass fiber and aqueous 2 M $ZnSO_4$ were used as the separator and electrolyte, respectively. The charge/discharge of cells was measured on a battery-testing instrument (LandHe, Wuhan, China; NEWARE, Shenzhen, China). Cycling stability of different Zn electrode were measured using Zn||Zn symmetric cells.

The activated carbon (AC) cathode was prepared by blending the slurry mixture of AC, acetylene black, and polytetrafluoroethylene in a mass ratio of 8:1:1 using water as the solvent onto a Ti grid, and then was dried at 60 ^{o}C for 12 h under vacuum, and the typical mass loading of the as-prepared cathode is ~2 mg cm^{-2}; The pyrene-4,5,9,10-tetraketone (PTO) cathode material was prepared by blending the slurry mixture of PTO, Ketjen black, and polytetrafluoroethylene in a mass ratio of 6:3:1 using water as the solvent onto a Ti grid, and then was dried at 60 ^{o}C for 12 h under vacuum, and the typical mass loading of the as-prepared cathode is ~5 mg cm^{-2}; The full cells of AC||Zn cell and PTO||Zn were tested in the range of 0-1.95 V and 0.36-1.46 V, respectively. The specific capacity and current density were calculated based on the mass of active material.

Cyclic voltammetry (CV) curves, linear scan voltammetry (LSV), chronoamperometry (CA), were carried out on a SP-300 electrochemical workstation (Bio-Logic, France). CV curves were measured at scan rate of 2 mV s^{-1} using a three electrode system with Zn as working electrode and counter electrode, Ag/AgCl as reference electrode. HER were measured using LSV measurement at scan rate at 5 mV s^{-1} by using Zn as working electrode, Ti as counter electrode and Ag/AgCl as reference electrode. To prevent the reduction of Zn^{2+} from affecting HER testing, 1 M $ZnSO_4$ was chosen as the electrolyte. Chronoamperometry (CA) measurements were carried out at a constant potential of −200 mV using Zn||Zn symmetric cell.

DFT calculations

Spin-polarized density functional theory (DFT) calculations were performed using the Vienna ab initio Simulation Package (VASP)[2,3]. The core electrons were described using the projected augmented wave (PAW) method[4,5], and the electron interactions were treated by the Perdew-Burke-Ernzerhof (PBE) exchange-correlation functional within the generalized gradient approximation (GGA)[6], with a plane-wave cutoff energy of 400 eV. The dispersion correction in Grimme's scheme was considered using DFT-D3 method[7]. Four layers of Zn(200), Zn(100), and Zn(101) were constructed as the slab model. For the geometry optimization, the top three layers of atoms were relaxed completely, whilst the bottom one layer of atoms were fixed. The Brillouin zone was sampled with Γ-point-centered Monkhorst-Pack k-point grid of 3×3×1. The energy and force convergence thresholds were set to be 1×10−6 eV and 0.05 eV Å−1, respectively. A vacuum space of 20 Å in the c direction for all Zn surface models was applied to avoid interactions between mirror images. Due to its simplicity and low computational costs, VASPsol was used to in our electrochemical systems for calculating the implicit solvation effect, where the dielectric constant of water is 80 (EB_k = 80)[8,9].

The adsorption energy was calculated using the following equation[10-12]:

$$E_{ads} = E(system) - E(slab) - E(adsorbent) \quad (1)$$

where E(system), E(slab), E(adsorbent) represent the total electronic energy of the optimized system, Zn surface slab, isolated adsorbent molecule.

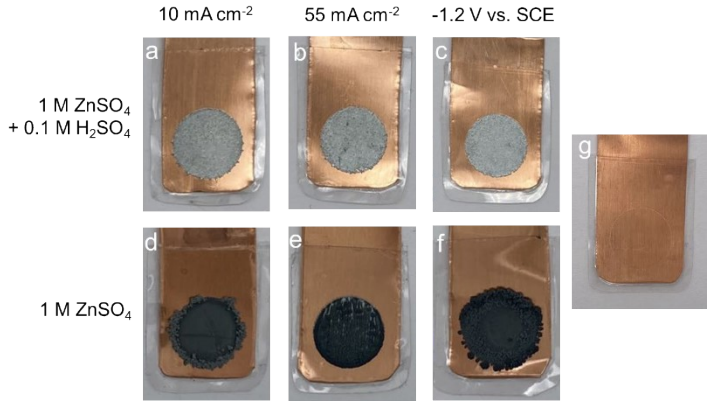

Figure S1. (a-f) Digital photos of the deposited zinc (40 mAh cm^{-2}) on Cu substrate using different deposition procedures (galvanostatic deposition at 10 mA cm^{-2}, 55 mA cm^{-2}, and potentiostatic deposition at −1.2 V vs. SCE) in 1 M $ZnSO_4$ electrolyte with or without 0.1 M H_2SO_4 additive. (g) Digital photos of bare Cu electrode with 1 cm^2 area exposed for electroplating.

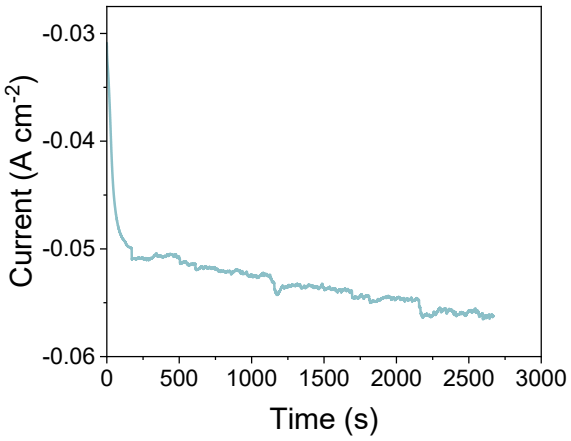

Figure S2. Corresponding time-current curve during potentiostatic deposition of zinc at −1.2 V vs. SCE in electrolyte with H_2SO_4 additive.

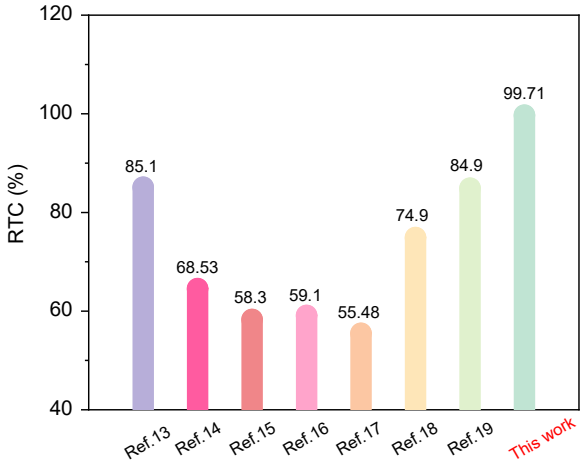

Figure S3. RTCs comparison of Zn(002) with others references.

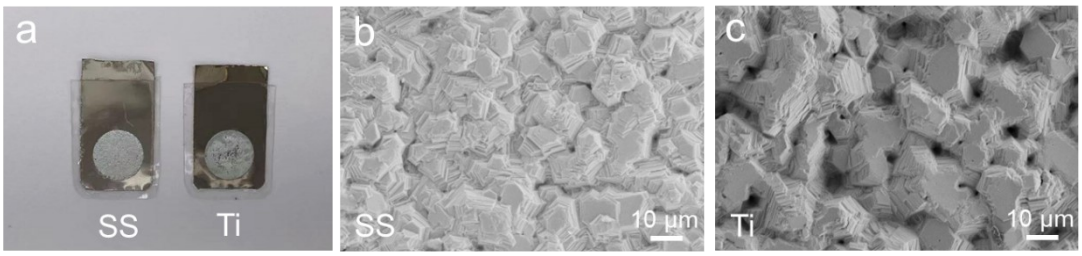

Figure S4. Digital photos of the deposited zinc (40 mAh cm^{-2}) using potentiostatic deposition procedure on (a) SS and Ti substrate at −1.2 V vs. SCE in the electrolyte with H_2SO_4 additive. Corresponding SEM images on (b) SS and (c) Ti.

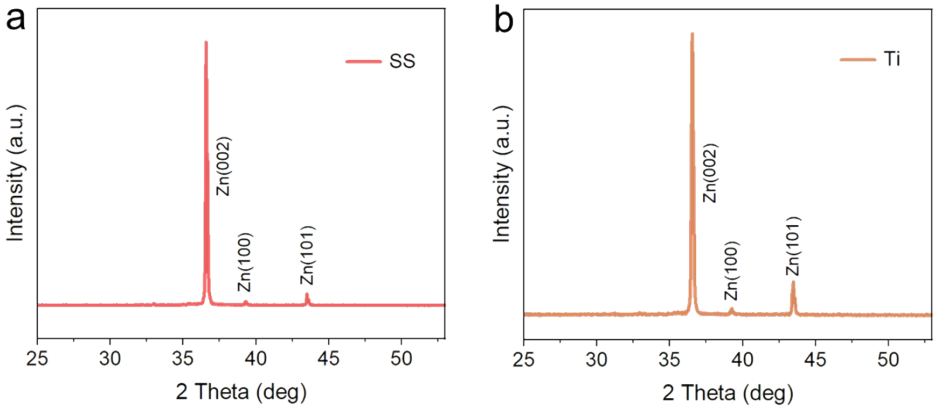

Figure S5. XRD patterns of the deposited zinc (40 mAh cm^{-2}) using potentiostatic deposition procedure on (a) SS and (b) Ti substrate at −1.2 V vs. SCE in the electrolyte with H_2SO_4 additive.

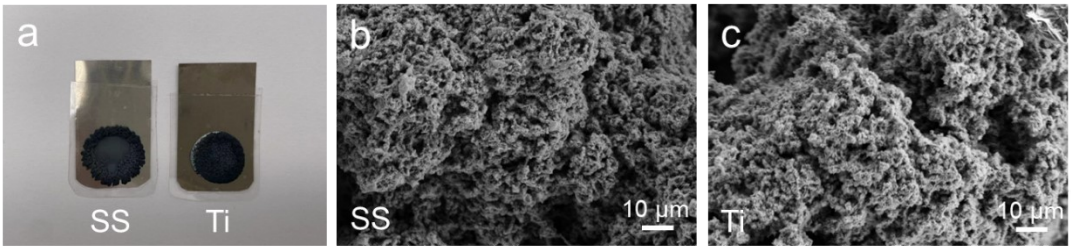

Figure S6. Digital photos of the deposited zinc (40 mAh cm^{-2}) using potentiostatic deposition procedure on (a) SS and Ti substrate at −1.2 V vs. SCE in the electrolyte without H_2SO_4 additive. Corresponding SEM images on (b) SS and (c) Ti.

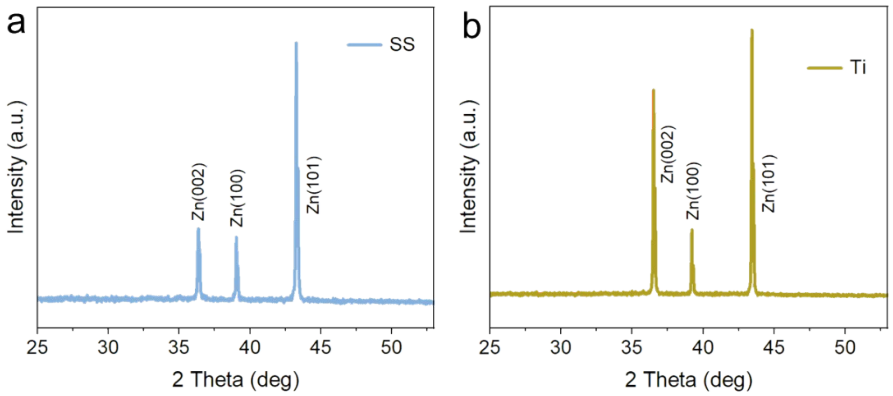

Figure S7. XRD patterns of the deposited zinc (40 mAh cm^{-2}) using potentiostatic deposition procedure on (a) SS and Ti substrate at −1.2 V vs. SCE in the electrolyte without H_2SO_4 additive.

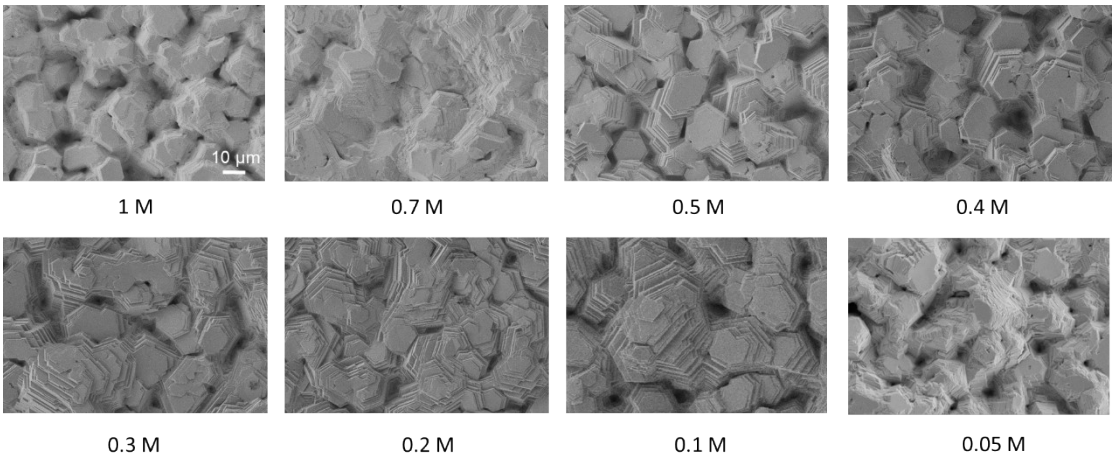

Figure S8. SEM images of deposited zinc (40 mAh cm^{-2}) using potentiostatic deposition procedure on Cu substrate at −1.2 V vs. SCE in the electrolyte with different concentration of H_2SO_4 additive from 0.05 M to 1M.

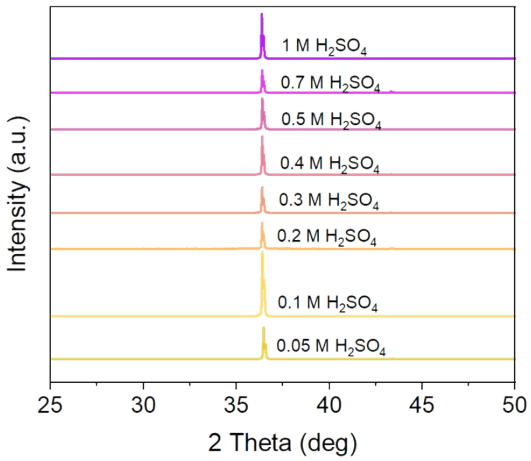

Figure S9. XRD patterns of deposited zinc (40 mAh cm^{-2}) using potentiostatic deposition procedure on Cu substrate at −1.2 V vs. SCE in the electrolyte with different concentration of H_2SO_4 additive from 0.05 M to 1M. When the concentration of H_2SO_4 is 0.1 M, obtained Zn(002) shows the highest peak intensity. When the concentration is lower than 0.1 M, the adsorption of H^+ is insufficient, thus leading to weak co-charge repulsion, resulting in the lower peak intensity of Zn(002). On the other hand, when the proton concentration is too high, the adsorption of protons on Zn(002) plane will be saturated, and excess protons will adsorb on others crystal face, which is not conducive to the formation of Zn(002) texture.

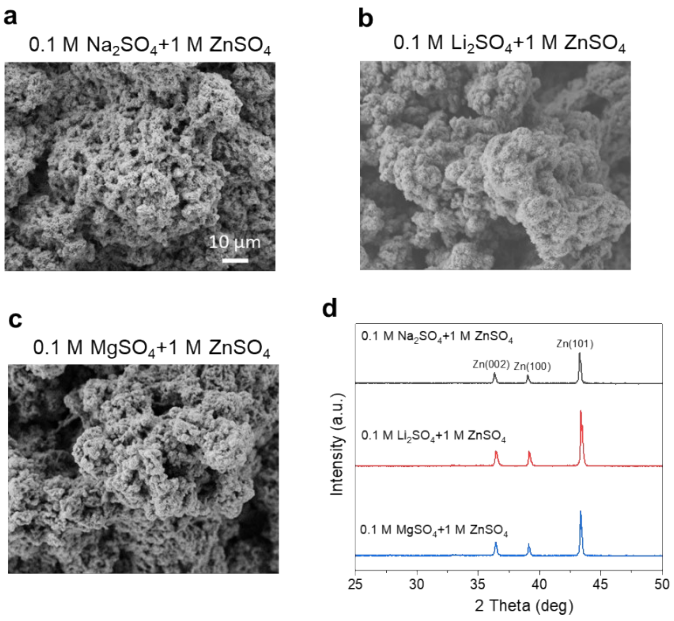

Figure S10. SEM images of deposited zinc (40 mAh cm^{-2}) using potentiostatic deposition procedure on Cu substrate at −1.2 V vs. SCE in different electrolyte of (a) 0.1 M Na_2SO_4 + 1 M $ZnSO_4$, (b) 0.1 M Li_2SO_4 + 1 M $ZnSO_4$, (c) 0.1 M $MgSO_4$ + 1 M $ZnSO_4$, (d) corresponding XRD patterns of deposited Zn in electrolyte with Na^+, Li^+ and Mg^{2+} additives.

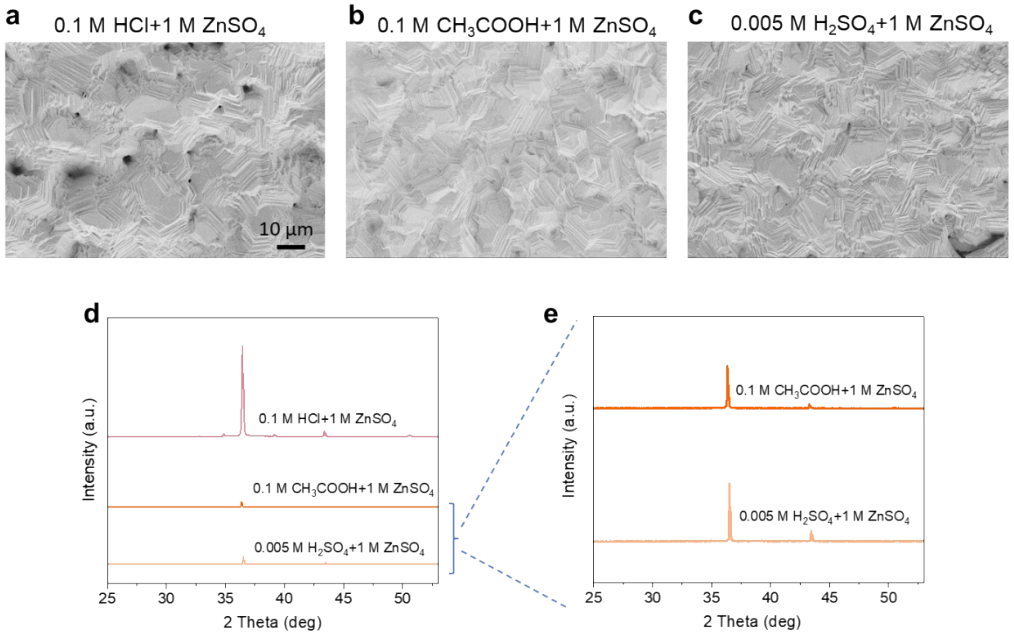

Figure S11. SEM images of deposited zinc (40 mAh cm^{-2}) using potentiostatic deposition procedure on Cu substrate at −1.2 V vs. SCE in different electrolyte of (a) 0.1 M HCl + 1 M $ZnSO_4$, (b) 0.1 M CH_3COOH + 1 M $ZnSO_4$, (c) 0.005 M H_2SO_4 + 1 M $ZnSO_4$, and (d) corresponding XRD patterns of deposited Zn. (e) enlarged view of XRD patterns for deposited Zn in 0.1 M CH_3COOH + 1 M $ZnSO_4$ and 0.005 M H_2SO_4 + 1 M $ZnSO_4$, respectively.

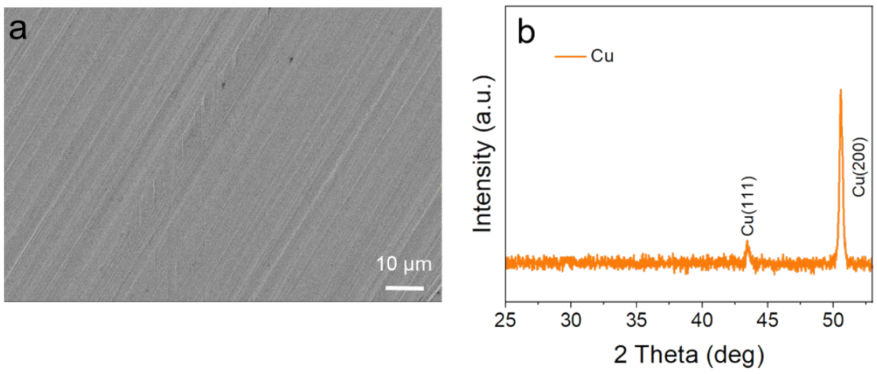

Figure S12. SEM and XRD patterns of bare Cu substrate.

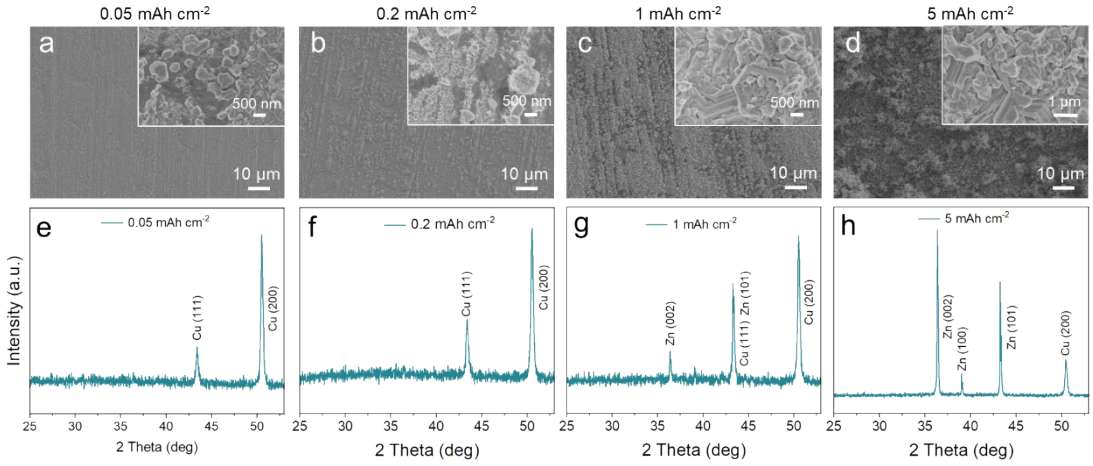

Figure S13. (a-d) SEM images and corresponding (e-h) XRD patterns of deposited Zn with different deposition capacities in 1 M $ZnSO_4$ electrolyte using potentiostatic deposition procedure at −1.2 V vs. SCE.

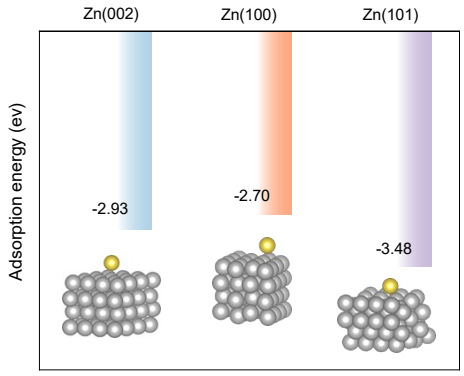

Figure S14. Adsorption energies of Na^+ on Zn(002), Zn(001) and Zn(101) crystallographic plane.

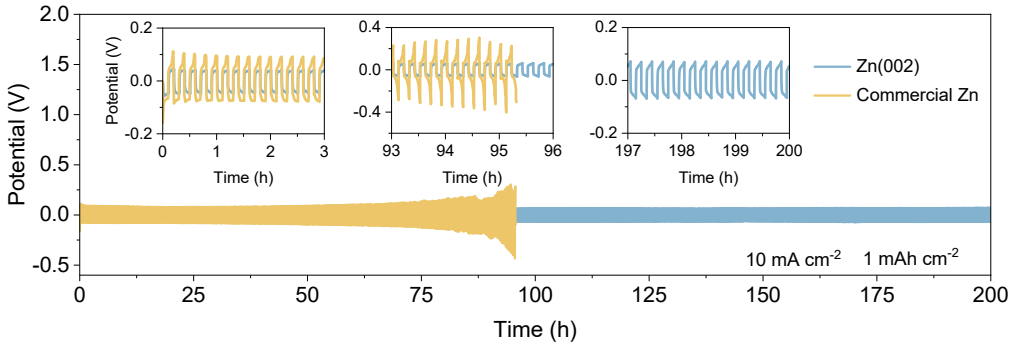

Figure S15. Comparison of galvanostatic cycling of Zn||Zn-symmetric cell using Zn(002) and commercial Zn electrode in 2 M $ZnSO_4$ at 10 mA cm^{-2} with 1 mAh cm^{-2}.

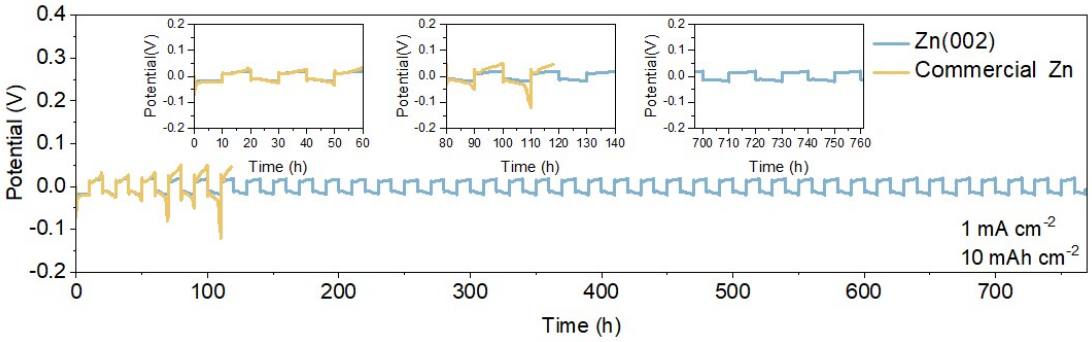

Figure S16. Comparison of long-term galvanostatic cycling of Zn||Zn-symmetric cell using Zn(002) and commercial Zn electrode in 2 M $ZnSO_4$ at 1 mA cm^{-2} with 10mAh cm^{-2}.

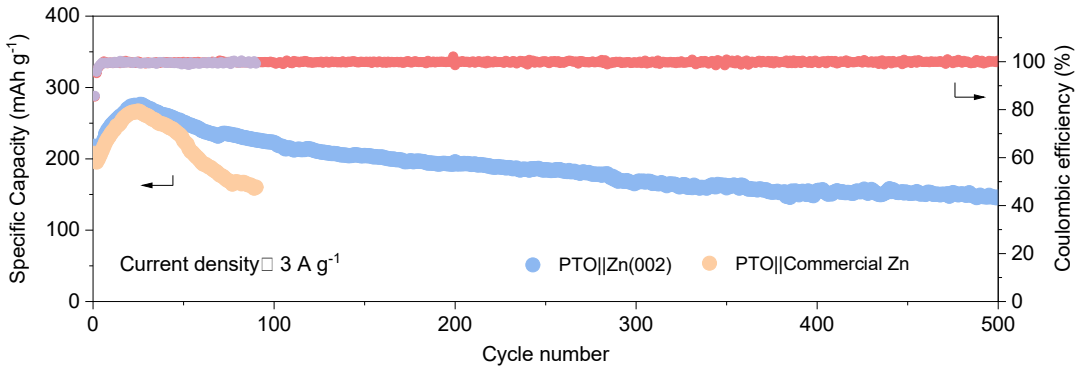

Figure S17. Long-term cycling performance for PTO||Zn full cell with high mass loading of 10 mg cm^{-2} at a current density of 3 A g^{-1}.

Table S1. RTCs comparison of Zn(002) with others references

Reference number	Improvement approach	RTC
1 Ref.13	disodium maleate additive	85.1%
2 Ref.14	thiamine hydrochloride additive	68.53%
3 Ref.15	glycine additive	58.3%
4 Ref.16	1-butyl-3-methylimidazolium ion additive	59.1%
5 Ref.17	(dimethyl(methacryloyloxyethyl) ammonium propane sulfonate additive	55.48%
6 Ref.18	Ag-modified surface	74.9%
7 Ref.19	High current density	84.9%
This work	Proton additive	99.71%

Table S2. Cumulative cycling capacity of symmetrical cells in different references

Reference number	Current (mA cm^{-2})/Capacity (percycle, mAh cm^{-2})	Time (h)	Cumulative capacity (mAh cm^{-2})
1 Ref.13	1/1	3200	1600 mAh cm^{-2}
2 Ref.14	5/5	1600	4000 mAh cm^{-2}
3 Ref.15	1/1	3100	1550 mAh cm^{-2}
4 Ref.16	1/0.5	3200	1600 mAh cm^{-2}
5 Ref.17	5/5	550	1375 mAh cm^{-2}
6 Ref.18	5/5	110	275 mAh cm^{-2}
7 Ref.19	2/2	500 h	500 mAh cm^{-2}
8 Ref.20	5/5	200 h	500 mAh cm^{-2}
9 Ref.21	2.5/2.5	2500 h	3125 mAh cm^{-2}
10 Ref.22	5/2.5	500 h	1250 mAh cm^{-2}
11 Ref.23	5/5	500 h	1250 mAh cm^{-2}
12 Ref.24	5/5	1000 h	2500 mAh cm^{-2}
13 Ref.25	10/5	700 h	3500 mAh cm^{-2}
14 Ref.26	2/2	1750 h	1750 mAh cm^{-2}
15 Ref.27	10/5	450 h	2250 mAh cm^{-2}
This work	5/5	1900 h	4750 mAh cm^{-2}

References

1. Z. Guo, Y. Ma, X. Dong, J. Huang, Y. Wang and Y. Xia, *Angewandte Chemie International Edition*, 2018, **57**, 11737-11741.
2. G. Kresse and J.Hafner, *Physical Review B*, 1993, **47**, 558-561.
3. G. Kresse and J. Hafner, *Physical Review B*, 1994, **49**, 14251-14269.
4. P. E. Blöchl, *Physical Review B*, 1994, **50**, 17953-17979.
5. G. Kresse and D. Joubert, *Physical Review B*, 1999, **59**, 1758-1775.
6. J. P. Perdew, K. Burke and M. Ernzerhof, *Physical Review Letters*, 1996, **77**, 3865-3868.
7. S. Grimme, *Journal of Computational Chemistry*, 2006, **27**, 1787-1799.
8. K. Mathew, V. S. C. Kolluru, S. Mula, S. N. Steinmann and R. G. Hennig, *Journal of Chemical Physics*, 2019, **151**, 234101.
9. K. Mathew, R. Sundararaman, K. Letchworth-Weaver, T. A. Arias and R. G. Hennig, *Journal of Chemical Physics*, 2014, **140**, 084106.
10. X. Liu, Y. Jiao, Y. Zheng, K. Davey and S.Z. Qiao, *Journal of Materials Chemistry A* 2019, **7**, 3648-3654.
11. D. Xu, X. Long, J. Xiao, Z. Zhang, G. Liu, H. Tong, Z. Liu, N. Li, D. Qian, J. Li and J. Liu, *Chemical Engineering Journal*, 2021, **422**, 129982.
12. Y. Li, H. Su, S. H. Chan, and Q. Sun, *ACS Catalysis*, 2015, **5**, 6658-6664.
13. T. Wei, H. Zhang, Y. Ren, L. Mo, Y. He, P. Tan, Y. Huang, Z. Li, D. Zhu and L. Hu, *Advanced Functional Materials*, 2024, **34**, 2312506.
14. S. Hu, H. Tao, H. Ma, B. Yan, Y. Li, L. Zhang and X. Yang, *ACS Applied Materials & Interfaces*, 2024, **16**, 18949−18958.
15. X. Liang, X. Chen, Z. Zhai, R. Huang, T. Yu and S. Yin, *Chemical Engineering Journal*, 2024, **480**, 148040.
16. C. Fan, W. Meng, J. Han, T. Li, D. Zuo, S. Deng, D. Li and L. Jiang, *Energy Storage Materials*, 2024, **71**, 103554.
17. S. Zhou, X. Meng, Y. Chen, J. Li, S. Lin, C. Han, X. Ji, Z. Chang and A. Pan, *Angewandte Chemie Int ernational Edition*, 2024, **136**, e202403050.
18. X. Zhou, B. Wen, Y. Cai, X. Chen, L. Li, Q. Zhao, S. Chou and F. Li, *Angewandte Chemie Int ernational Edition*, 2024, **63**, e202402342.
19. J. Zhang, W. Huang, L. Li, C. Chang, K. Yang, L. Gao, X. Pu, *Advanced materials*, 2023, **35**, 2300073.
20. M. Zhou, S. Guo, J. Li, X. Luo, Z. Liu, T. Zhang, X. Cao, M. Long, B. Lu, A. Pan, G. Fang, J. Zhou, S. Liang, *Advanced Materials*, 2021, **33**, 2100187.
21. J. Ji, Z. Zhu, H. Du, X. Qi, J. Yao, H. Wan, H. Wang, L. Qie, Y. Huang, *Advanced Materials*, 2023, **35**, 2211961.
22. J. Cao, D. Zhang, C. Gu, X. Wang, S. Wang, X. Zhang, J. Qin, Z. S. Wu, *Advanced Energy Materials*, 2021, **11**, 2101299.
23. Y. Hao, D. Feng, L. Hou, T. Li, Y. Jiao, P. Wu, *Advanced Science*, 2022, **9**, 2104832.
24. D. Feng, Y. Jiao, P. Wu, *Angewandte Chemie International Edition*, 2023, **62**. e202314456.
25. X. Song, L. Bai, C. Wang, D. Wang, K. Xu, J. Dong, Y. Li, Q. Shen, J. Yang, *ACS Nano*, 2023, **17**, 15113-15124.
26. M. Peng, X. Tang, K. Xiao, T. Hu, K. Yuan, Y. Chen, *Angewandte Chemie International Edition*, 2023, **62**, e202302701
27. T. Li, S. Hu, C. Wang, D. Wang, M. Xu, C. Chang, X. Xu, C. Han, *Angewandte Chemie International Edition*, 2023, **62**, e202314883.